AGU PUBLICATIONS

Geophysical Research Letters

RESEARCH LETTER
10.1002/2016GL070589

**Key Points:**
- Seven years of satellite-derived glacier frontal ablation are used to develop models that estimate weekly frontal ice loss from seismic data
- Duration of seismic calving signals and catalog incompleteness mainly controlled by seismic noise level are suitable predictor variables
- Frontal ablation from Kronebreen reveals sharp summer increase, short-lived effects of rainfall events, and characteristic decay in autumn

**Supporting Information:**
- Supporting Information S1
- Data Set S1
- Data Set S2

**Correspondence to:**
A. Köhler,
andreas.kohler@geo.uio.no

**Citation:**
Köhler, A., C. Nuth, J. Kohler, E. Berthier, C. Weidle, and J. Schweitzer (2016), A 15 year record of frontal glacier ablation rates estimated from seismic data, *Geophys. Res. Lett.*, *43*, 12,155–12,164, doi:10.1002/2016GL070589.

Received 26 JUL 2016
Accepted 15 NOV 2016
Accepted article online 21 NOV 2016
Published online 15 DEC 2016



# A 15 year record of frontal glacier ablation rates estimated from seismic data

**Andreas Köhler[1], Christopher Nuth[1], Jack Kohler[2], Etienne Berthier[3], Christian Weidle[4], and Johannes Schweitzer[1,5]**

[1]Department of Geosciences, University of Oslo, Oslo, Norway, [2]Norwegian Polar Institute, Polar Environmental Centre, Tromsø, Norway, [3]LEGOS, Université de Toulouse, CNRS, CNES, IRD, UPS, Toulouse, France, [4]Institute of Geosciences, Kiel University, Kiel, Germany, [5]NORSAR, Kjeller, Norway

**Abstract** We present a unique time series of continuous glacier frontal ablation rates with weekly resolution over 15 years estimated from seismic calving observations at Kronebreen, Svalbard. Using linear statistical models, we calibrate the seismic record with 7 years of satellite-derived frontal ablation measurements. The two basic input parameters required for our models are the cumulative duration of individual seismic calving events and the incompleteness of the seismic record to correct for the effect of seismic background noise. Frontal ablation follows the seasonal glacier speedup, peaking 1–2 months after the melt season maximum. Short-lived peaks are associated with melt and rain events. Cumulative frontal ablation of Kronebreen between 2001 and 2015 is about 4.0 $km^3$ (3.7 Gt), with the greatest annual loss (0.45 $km^3$) between 2013 and 2014 at the onset of the recent accelerated retreat of the glacier. Our approach provides a potential method for monitoring tidewater glaciers worldwide that have sufficiently close seismic instrumentation.

## 1. Introduction

Dynamic ice loss through glacier calving contributes significantly to eustatic sea level rise in a warming climate [*Vaughan et al.*, 2013; *Gardner et al.*, 2013; *Huss and Hock*, 2015]. To better understand controls on calving processes and to further improve models that predict glacier mass changes through time, high temporal resolution in situ observations of calving are required [*Benn et al.*, 2007; *Vieli and Nick*, 2011]. Such observations of calving include human observation, time-lapse imagery, and ground-based radar surveillance [e.g., *O'Neel et al.*, 2003; *Chapuis et al.*, 2010]. However, these records are of limited time span. Repeat satellite imagery allows measurement of glacier velocity and changes in terminus position. Provided ice thickness is known at the glacier front, these data can be used to estimate the total ice volume flux at the terminus [*Mansell et al.*, 2012; *Schellenberger et al.*, 2015], i.e., frontal ablation as defined by *Cogley et al.* [2011]. However, temporal resolution is limited to weeks, months or years, which is too low to capture the fine scale processes and feedbacks occurring at the ocean-glacier-atmosphere boundaries. Alternatively, passive seismic glacier monitoring is able to capture calving [*Qamar*, 1988; *Ekström et al.*, 2003; *Amundson et al.*, 2008; *Richardson et al.*, 2010; *O'Neel et al.*, 2010; *Walter et al.*, 2012; *Köhler et al.*, 2012; *Bartholomaus et al.*, 2012; *Köhler et al.*, 2015; *Podolskiy and Walter*, 2016], with the potential to provide high temporal resolution and long, continuous records being less affected by meteorological conditions and season (i.e., clouds and Arctic winter).

Seismic instruments capture calving indirectly through ground shaking recorded at a wide range of distances. Background seismic noise and attenuation of seismic wave amplitudes hinder detection of small and distant calving events. Therefore, simultaneous direct calving observations are required for calibration, i.e., to relate seismic signal properties and ice volumes of individual calving events [*Qamar*, 1988; *O'Neel et al.*, 2007b; *Bartholomaus et al.*, 2012] and to assess the record completeness. A first calibrated model to estimate ice loss from seismic data has recently been published for the Yahtse glacier, Alaska [*Bartholomaus et al.*, 2015].

We pursue a novel approach to estimate frontal ablation from passive seismic records by developing and calibrating a statistical model with ablation rates from satellite data of varying resolution from weeks to months. Hence, no observed ice volumes of individual calving events are required, and subaerial and subaqueous frontal melting is accounted for. Our study focuses on Kronebreen, a tidewater glacier on the Arctic archipelago of Svalbard (74–81°N, 10–35°E, Figure 1).

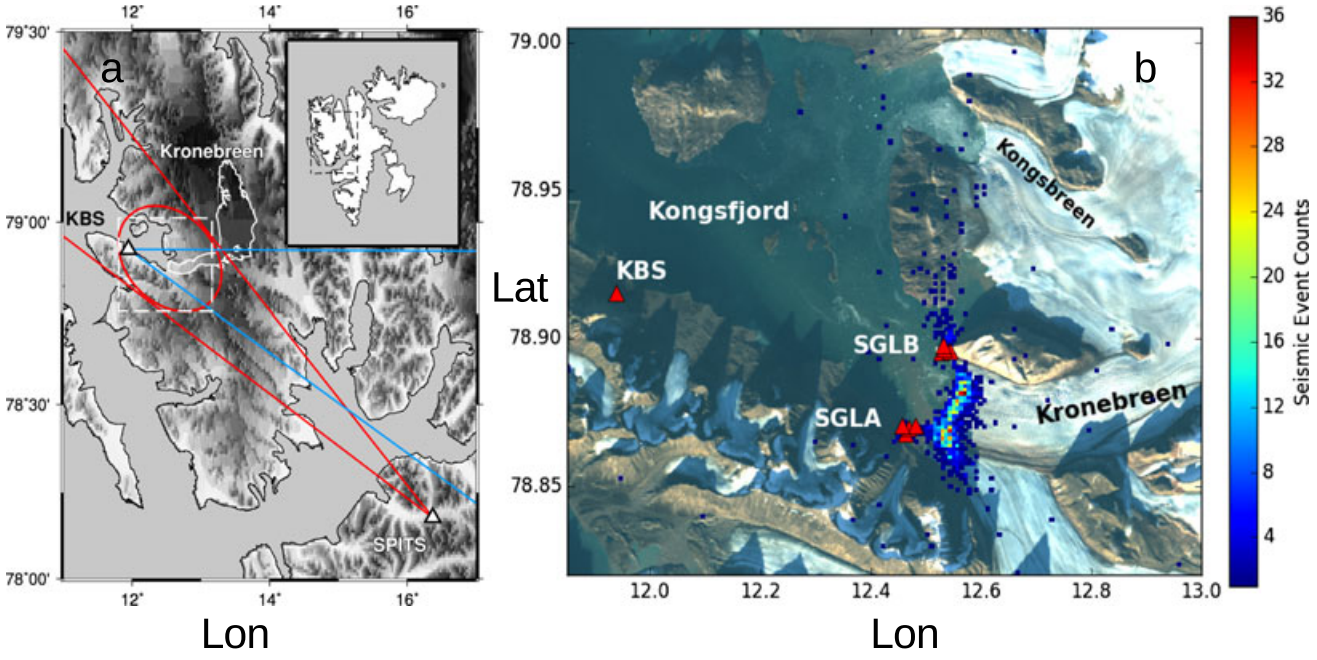


**Figure 1.** (a) Map of Svalbard with Kronebreen (white line) and area shown in Figure 1b (white dashed box). Red and light blue lines and ellipse illustrate the empirical classification method to detect Kronebreen calving events using seismic data from the permanent Kings Bay seismic station (KBS) and the permanent small-aperture Spitsbergen seismic array (SPITS) (white triangles). Directional information is obtained from seismic signal polarization on KBS (light blue) and frequency-wave number analysis on SPITS (red), and distance proportional information from traveltime difference between SPITS and KBS (sketched by red ellipse). (b) Relocation of Kronebreen events detected at KBS/SPITS (Catalog 2) between May and August 2013 with local, temporary arrays SGLA and SGLB, showing the reliability of calving detections.

On Svalbard 68% of the glacier area drains through over 170 tidewater glacier marine fronts [*Nuth et al.*, 2013]. In northwest Svalbard, close to the Ny Ålesund research base, (Figure 1) lies Kronebreen, a large (~400 km$^2$) continuously fast-flowing tidewater glacier with an average annual frontal velocity of 1–3 m/d [*Voigt*, 1966; *Kääb et al.*, 2005; *Schellenberger et al.*, 2015]. The total glacier mass loss between 1966 and 2007 amounts to about 8 km$^3$ WE, of which frontal ablation accounts for 6.7 km$^3$ WE [*Nuth et al.*, 2012]. The glacier front position had been stable since 1990 but recently entered a phase of retreat, ~1 km from January 2013. Two permanent seismic broadband stations record calving at Kronebreen: the Kings Bay seismic station (KBS) in Ny Ålesund at about 15 km distance and the small-aperture Spitsbergen seismic array (SPITS) close to Longyearbyen at about 115 km distance from the glacier front.

## 2. Data

### 2.1. Seismic Calving Record

Analysis of regional seismicity on Svalbard reveals a high number of seismic signals related to glacier dynamic activity across the archipelago [*Köhler et al.*, 2015]. Most events result from calving at tidewater glaciers and are characterized by narrowband signals with spectral peaks between 1 and 8 Hz, similar to those observed in Alaska and Greenland [*O'Neel and Pfeffer*, 2007a; *Amundson et al.*, 2008; *Richardson et al.*, 2010; *Bartholomaus et al.*, 2012]. These events are characterized by mostly emergent signal onsets, ambiguous phase arrivals, and high waveform variability when recorded close to the source. This is a result of the complex seismic source related to iceberg-sea surface interactions such as underwater iceberg deceleration and air cavity collapse after the iceberg impact in the water [*Bartholomaus et al.*, 2012].

We use continuous seismic data of KBS and SPITS recorded between 2001 and 2015 (Figure 1a) to automatically detect calving events at Kronebreen. The calving signal properties described above and the sparse character of the regional seismic network prevents a precise, deterministic location of most events. We therefore adapt the empirical detection method introduced in *Köhler et al.* [2015]. A short-term/long-term trigger algorithm (STA/LTA) in the calving frequency band (1–8 Hz) is applied at KBS. For each detection the average or effective polarization direction of the seismic signal at KBS is estimated [*Flinn*, 1965] and used to determine the direction toward the event source [*Asming and Fedorov*, 2015]. Using the SPITS array, additional event

features are computed through frequency-wavenumber (FK) analysis [*Ohrnberger et al.*, 2004], i.e., wave propagation direction and *P-S* travel time difference. Subsequently, a naïve Bayes classifier [*Bishop*, 2006; *Asming et al.*, 2015] is applied to all event features to select events most likely originating at Kronebreen. We describe the detector and how the classifier is trained using data of a temporary local seismic network in the supporting information (Text S2/S3).

To estimate frontal ablation at Kronebreen, we compile two seismic calving event catalogs: (1) Catalog 1: classified using polarization feature (KBS) and (2) Catalog 2: classified using polarization (KBS) and FK features (SPITS). Catalog 1 is more complete than Catalog 2 since KBS is closer to Kronebreen. However, since only a single station is used, the record is more prone to misclassifications from other tidewater glaciers or from nonglacier events with similar signal features. Catalog 2 includes only events large enough to be recorded at SPITS, but by using two stations the source location is much better constrained (Figure 1a). For each seismic event, we determine the duration, the maximum envelope amplitude, and the sum of signal envelope amplitudes over the duration of the event (duration amplitude).

Event misclassifications and variations in the seismic background noise affect the quality and completeness of the seismic calving record. Weak seismic signals related to small pieces of ice or submarine calving [*Bartholomaus et al.*, 2012; *Köhler et al.*, 2015] are missed by the STA/LTA detector as background noise increases, and polarization/array analysis results may be biased due to noisy data. To show that our seismic catalogs are indeed robust and reliable records of calving seismicity at Kronebreen, we use a local seismic data set recorded between May and August 2013 less than 1 km from the terminus of Kronebreen (two geophone arrays, Text S1). More precise event locations obtained with the local data clearly outline the terminus (Figure 1b) [*Koubova*, 2015]. Furthermore, temporal variability is highly correlated between Catalogs 1, 2, and an independent record of calving events detected on the local arrays (Catalog 3 and Figure S2 and Text S4). Moreover, seismic background noise must be considered because it is partially anticorrelated with the seismic event rate (Figure S2 and Text S4).

Different quantities to indicate variations in the seismic noise level are computed: the daily averaged envelope amplitude at KBS ($N_1$) and SPITS ($N_2$) in the frequency band 2–10 Hz (STA/LTA triggered events are removed), and an evaluation of the incompleteness of the seismic catalog through the ratio between large and small events:

$$N_3 = (\log(n(M \geq 0.8)) - \log(n(M < 0.8)) + 2)^{1.5}, \quad (1)$$

where $n(M \geq 0.8)$ and $n(M < 0.8)$ are the number of events above and below the seismic magnitude threshold of $M = 0.8$ per time interval. A higher noise level will result in fewer detections below $M = 0.8$ and, thus, in a larger $N_3$ indicating a less complete catalog. Using $N_3$ is plausible because calving volumes and seismic event magnitudes at Kronebreen both follow power law distributions (Figure S3) [*Chapuis and Tetzlaff*, 2014; *Åström et al.*, 2014]. However, magnitude-range-dependent deviations from the power law distribution may exist for seismic calving events [*Bartholomaus et al.*, 2015]. For more details on magnitude determination, magnitude frequency distribution, and $N_3$ we refer to the supporting information (Texts S3 and S4) [*Ogata and Katsura*, 1993; *Woessner and Wiemer*, 2005].

### 2.2. Frontal Ablation Rates

Seismic calving observables are calibrated with satellite remote sensing observations. We estimate 2007–2013 Kronebreen frontal ablation rates ($\dot{A}$) from FORMOSAT-2 satellite optical imagery (2 m resolution) at 2–5 week intervals during the Arctic summer (timing dependent on cloud-free days) and once over the Arctic winter. Images were orthorectified using ground control points extracted manually on a September 2007 SPOT-5 orthoimage and digital elevation model [*Korona et al.*, 2009]. Standard image matching techniques using Cosi-CORR [*Leprince et al.*, 2007] were applied to sequential imagery to derive velocity fields of the glacier tongue. The velocity was integrated across a flux gate at the front of Kronebreen and combined with the map of the bedrock topography (J. Kohler, unpublished data, 2015) to generate ice flux through the gate ($U_{fx}$). Block flow that is assumed as internal deformation is inferred as less than 5% of the total speed higher up on the glacier [*Bahr*, 2015]. Glacier front positions were manually digitized from the imagery and volumetric changes of the terminus ($dl/dt$) were summed with ice flux through the gate to generate frontal ablation rates:

$$\dot{A} = U_{fx} + dl/dt. \quad (2)$$

In this formulation, ice discharge out of the system is positive such that $+dl/dt$ indicates retreat and $-dl/dt$ advance of the terminus.

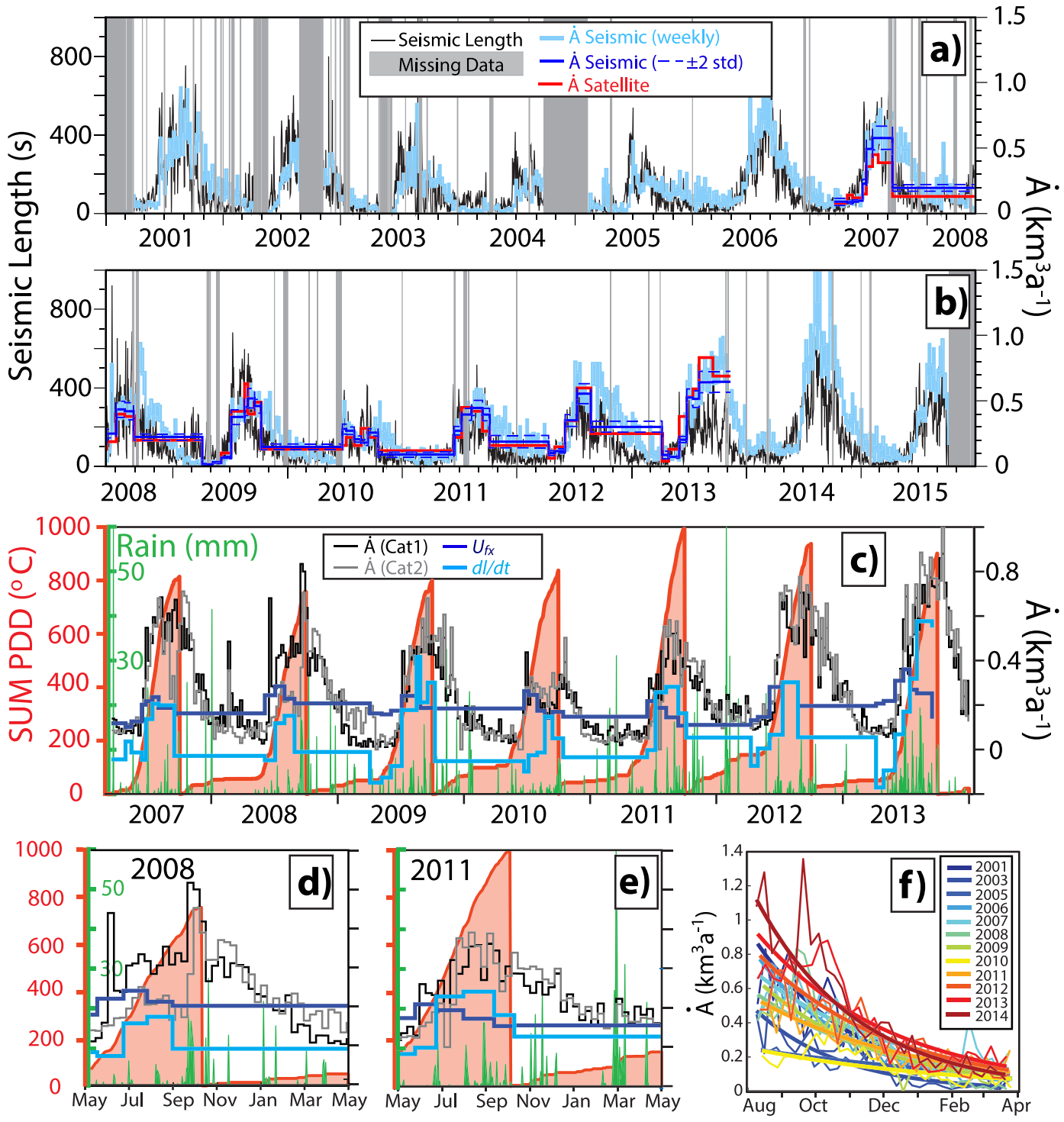


**Figure 2.** (a and b) Seismically observed calving (black) and estimated frontal ablation rates ($\dot{A}$) from satellite data (red) and seismic observations (blue, dashed line is ±2 standard deviations) at Kronebreen for Catalog 1. "Seismic length" is cumulative duration of all calving signals per day in seconds. Light blue colors show the weekly estimated ablation rates for the entire period. Line thickness represents model uncertainty (two times prediction standard deviation). Light gray areas indicate seismic data gaps. (c) Comparison of $\dot{A}$ estimated from seismic data (Catalogs 1 and 2) with cumulative temperatures at positive degree days (PDDs) until October, rain, dynamic ($U_{fx}$) and front position components ($dl/dt$) of the satellite-derived $\dot{A}$. (d and e) Close-ups of Figure 2c. (f) Exponential decay functions fit to the decrease of $\dot{A}$ in autumn and winter.

## 3. Transferring Seismic Observations to Frontal Ablation Rates

We apply and calibrate generalized linear models (GLMs) [*McCullagh and Nelder*, 1989] to transfer the accumulated seismic calving event catalogs to the lower temporal resolution satellite frontal ablation rates. GLMs have been used previously to relate seismic signal attributes of individual calving events to ice volumes [*Bartholomaus et al.*, 2015]. In a GLM, the linear combination of predictor variables and the response variable (frontal ablation rate $\dot{A}$) is related through a link function. Here the predictor variables are the previously defined noise indicators $N_j$ ($j = 1, 2, 3$) and the following seismic calving rate variables $S_i$ determined for time periods of length $t$: $S_1$ = (event counts/$t$), $S_2$ = (sum of maximum event amplitudes/$t$), $S_3$ = (sum of event duration amplitudes/$t$), $S_4$ = (sum of event durations/$t$). GLMs support different distribution models for the response variable. Since negative calving flux is not physically possible, frontal ablation rate errors are not normally distributed with a constant variance [*Bartholomaus et al.*, 2015]. We find the gamma distribution and the identity link function to be most suitable for our models. Our final GLMs have the form:

$$\dot{A} = c_1 \cdot S_i \cdot N_j + c_2 \cdot N_k + c_0, \tag{3}$$

where $c_{0,1,2}$ are the time-invariant model coefficients. The interaction between variables ($S_i \cdot N_j$) accounts for the fact that the fraction of unobserved seismic calving does not remain constant during periods with stable noise, when calving activity increases. Models without the noise and interaction terms are also evaluated.

Satellite-derived ablation rates contain variable time resolutions from 11 days to 9 months and are given in units of $km^3\ a^{-1}$ (red curves in Figure 2). Seismic rates $S_i$ are obtained by summing over all seismic calving observations (event counts, amplitudes, or durations) in the corresponding time period and normalizing by the length in years. For a robust fit we require the deviance of each GLM to be lower than the null deviance (see Text S5 and Table S2). In addition, mean root-mean-square (RMS) errors are evaluated through a cross-validation test. Models including the interaction term ($N_3 \cdot S_4$) and seismic event duration ($S_4$) perform best (Figure S5a, highlighted in Table S2). For Catalogs 1 and 2, $N_3$ is preferred in the interaction term ($c_1$). In $c_2$, $N_3$ is found best for Catalog 1 and $N_2$ for Catalog 2. Figure 2 or S4 shows that the estimated ablation rates (blue) fit the observations (red) within the prediction error. The best model fit is achieved for Catalog 1 with lowest RMS error and a deviance of 4.4 (null deviance is 25.4). Analysis of observed and modeled ablation rates for more tested GLMs (Figure S6) confirms the importance of including seismic noise indicators and, especially in case of Catalog 1, shows the need for the interaction term. Both steps reduce the misfit considerably as higher noise results in less detected events and shorter seismic durations [*Bartholomaus et al.*, 2015]. However, variability in $N_3$ does not dominate the variability of the $\dot{A}$ time series (Figure S7a).

The best GLM for each catalog is used to estimate $\dot{A}$ with weekly resolution for the entire seismic data set (light blue in Figures 2 and S4). Good correspondence exists between the estimated rates of Catalogs 1 and 2 in different time periods (black symbols in Figures S5b–S5d). The spread is comparable within and outside the calibration period (2007–2013). The prediction error (defined in Text S5) averaged over all weekly data points is of the order of $\pm 0.1\ km^3\ a^{-1}$, i.e., about 10% of $\dot{A}$ observed during summer. *Schellenberger et al.* [2015] independently estimated the total frontal ablation at Kronebreen from SAR velocity data between May 2012 and May 2013 as 0.22–0.27 Gt $a^{-1}$. This value is within the errors of our estimate of $0.30 \pm 0.06$ Gt $a^{-1}$ (sum of weekly estimates over same time period, ice density 0.917 g $cm^{-3}$).

## 4. Discussion

### 4.1. Reliability of the Model

We reproduced 7 years of satellite-derived frontal ablation rates consistently using seismic events recorded on a single station located 15 km away and on a seismic array more than 100 km away from the glacier. Hence, monitoring glacier frontal ablation is feasible using seismic stations located up to near-regional distances (100–300 km). Seismic instruments are only sensitive to dynamic ice mass loss, i.e., calving. Thus, this reproduction of satellite-derived frontal ablation suggests a stable relative contribution of subaerial and subaqueous frontal melting on average. However, our prediction error may represent variability of this ratio on shorter time scales.

The seismic detector was trained and validated by utilizing four months of data from a temporary seismic network in 2013. We assume that the character of seismic signals and their detectability do not change through time, apart from variations due to changing noise level. This assumption is likely valid since the position of the calving front had been stable until 2013. Since the retreat onset at Kronebreen, the increasing distance to

**Table 1.** Total Annual Frontal Ablation $A$ ($km^3$) Obtained From Summation of Weekly Modeled Ablation Rates $\dot{A}$ Over Two Time Periods: Each Glacier Mass Balance Year Starting in September (1) and Calendar Year (2) for Catalogs 1 (Cat1) and 2 (Cat2)[a]

| Time Period 1 (Sep–Aug) | A Cat1<br>A Cat2 | A Gap Cat1<br>A Gap Cat2 | Calibration | Time Period 2 (Jan–Dec) | A Cat1<br>A Cat2 | A Gap Cat1<br>A Gap Cat2 | Calibration |
|---|---|---|---|---|---|---|---|
| 2001/2002 | 0.24 ± 0.06 | 0.02 | – | 2001 | 0.25 ± 0.06 | 0.04 | – |
| | 0.25 ± 0.07 | 0.03 | | | 0.27 ± 0.07 | 0.04 | |
| 2002/2003 | 0.13 ± 0.03 | 0.10 | – | 2002 | 0.15 ± 0.04 | 0.10 | – |
| | 0.14 ± 0.05 | 0.11 | | | 0.16 ± 0.05 | 0.11 | |
| 2003/2004 | 0.122 ± 0.027 | 0.016 | – | 2003 | 0.15 ± 0.04 | 0.03 | – |
| | 0.17 ± 0.07 | 0.03 | | | 0.18 ± 0.05 | 0.04 | |
| 2004/2005 | 0.10 ± 0.04 | 0.10 | – | 2004 | 0.068 ± 0.016 | 0.084 | – |
| | 0.15 ± 0.09 | 0.11 | | | 0.11 ± 0.06 | 0.10 | |
| 2005/2006 | 0.25 ± 0.07 | 0 | – | 2005 | 0.14 ± 0.04 | 0.02 | – |
| | 0.25 ± 0.08 | 0 | | | 0.20 ± 0.09 | 0.02 | |
| 2006/2007 | 0.27 ± 0.06 | 0 | – | 2006 | 0.30 ± 0.07 | 0 | – |
| | 0.28 ± 0.08 | 0 | | | 0.32 ± 0.09 | 0 | |
| 2007/2008 | 0.29 ± 0.06 | 0 | 0.19 | 2007 | 0.30 ± 0.06 | 0 | – |
| | 0.21 ± 0.06 | 0.03 | | | 0.27 ± 0.06 | 0.02 | |
| 2008/2009 | 0.23 ± 0.05 | 0 | 0.20 | 2008 | 0.29 ± 0.06 | 0 | 0.20 |
| | 0.25 ± 0.07 | 0.01 | | | 0.21 ± 0.06 | 0.02 | |
| 2009/2010 | 0.20 ± 0.04 | 0.02 | 0.18 | 2009 | 0.21 ± 0.05 | 0.01 | 0.21 |
| | 0.22 ± 0.06 | 0.01 | | | 0.26 ± 0.07 | 0.01 | |
| 2010/2011 | 0.17 ± 0.04 | 0.01 | 0.19 | 2010 | 0.16 ± 0.04 | 0.01 | 0.15 |
| | 0.16 ± 0.05 | 0.01 | | | 0.16 ± 0.05 | 0.01 | |
| 2011/2012 | 0.29 ± 0.06 | 0 | 0.24 | 2011 | 0.21 ± 0.05 | 0.01 | 0.20 |
| | 0.31 ± 0.07 | 0 | | | 0.20 ± 0.06 | 0.01 | |
| 2012/2013 | 0.33 ± 0.07 | 0 | 0.31 | 2012 | 0.33 ± 0.07 | 0 | 0.26 |
| | 0.36 ± 0.09 | 0 | | | 0.36 ± 0.09 | 0 | |
| 2013/2014 | 0.43 ± 0.09 | 0 | – | 2013 | 0.36 ± 0.07 | 0 | 0.37 |
| | 0.46 ± 0.13 | 0 | | | 0.39 ± 0.10 | 0 | |
| 2014/2015 | 0.36 ± 0.08 | 0 | – | 2014 | 0.45 ± 0.10 | 0 | – |
| | 0.37 ± 0.11 | 0 | | | 0.48 ± 0.14 | 0 | |
| 2015/2016 | – | – | – | 2015 | 0.23 ± 0.06 | 0.07 | – |
| | – | – | | | 0.22 ± 0.07 | 0.08 | |

[a]Gap: correction for seismic data gaps assuming weekly $\dot{A}$ equivalent to the average $\dot{A}$ in the corresponding month over all years. Calibration: $A$ obtained from satellite measurements. Error estimates are double standard error (~95% confidence interval). Mean annual $A$ over all years in Cat1/Cat2 is 0.27/0.28 $km^3$ and in calibration period 0.27/0.27 $km^3$.

KBS may have decreased detectability of weaker events which may require recalibration of our model in the future using newer satellite data.

The seismic record includes misclassifications (in particular Catalog 1) due to the lack of a dense seismic network. Here we benefit from Kronebreen being the most dominant source of seismicity in the vicinity of KBS. While a stable or even a slightly varying number of misclassifications does not seem to strongly affect the estimated ablation rates, deviations might exist from events mistaken for Kronebreen calving. For example, in 2007/2008 the total volume obtained from Catalog 1 is 0.1 $km^3$ larger than the satellite-derived value (0.19 $km^3$), while Catalog 2 shows good agreement (Table 1 and Figures 2a and S4). Hence, temporal variability of Catalogs 1 and 2 should be interpreted jointly.

Our model is developed using satellite observed ablation rates with a resolution varying from 2 weeks to several months. Applying our model at daily resolution produces more inconsistencies between Catalogs 1

and 2 compared to the stable results at weekly resolution (Figures S5b–S5d), suggesting that the models are only valid at resolutions of at least 7 days. Furthermore, weekly modeled rates tend to slightly overestimate the cumulative total annual frontal ablation compared to the satellite data (Table 1). Although this bias is within the model errors, it becomes more significant when summing frontal ablation over several years. Using lower temporal resolution reduces the bias (Figure S7b), implying a more representative distribution of calving event volumes over longer time periods. Reasons for this may include the underlying assumption that calving event volumes are power law distributed, which requires a sufficient number of calving events for appropriate sampling. Direct observations of individual calving events on shorter timescales (time-lapse camera images and terrestrial radar) have to be incorporated to increase resolution down to daily or even hourly timescales [*Bartholomaus et al.*, 2015].

Our results confirm previous findings that the duration of seismic calving signals is a better predictor for ice calving volumes than for example the maximum amplitude [*Qamar*, 1988; *O'Neel et al.*, 2007b; *Bartholomaus et al.*, 2015]. Nevertheless, models using event counts without any signal properties produces similar low misfits compared to the duration in the case of Catalog 2 (Table S2). Since this catalog only includes the largest calving events, the scaling between events of different sizes seems to be less important here. Most importantly, our findings strongly suggest that the variability of the seismic catalog completeness must be incorporated into statistical models estimating frontal ablation to correct for the effect of seismic noise level variability on observed seismic calving detection rates.

### 4.2. Time Series of Frontal Ablation at Kronebreen

Kronebreen frontal ablation varies significantly at annual, monthly, and weekly scales. Annually, the flux ranges from 0.14 to 0.48 $km^3\ a^{-1}$ (Table 1), while at a weekly resolution, the flux can vary from 0.01 to 1.35 $km^3\ a^{-1}$ (Figure 2). The year 2010 featured an exceptionally low calving activity. Lower values in 2002 and 2004 are affected by longer seismic data gaps, and a correction term is provided in Table 1 assuming an average monthly rate obtained from all years. Years with highest frontal ablation are 2001, 2006, 2007, and all years from 2012 to 2015 (Figure 2) due to the current retreat of Kronebreen [*Schellenberger et al.*, 2015]. We observe that $N_3$ tends to increase on average since 2012, correlating well with the retreat of Kronebreen. This can be an effect of calving style (more large events) or of the increased distance to KBS (less small events detected and catalog less complete).

Figure 2c shows the seismic derived frontal ablation with the two components of the satellite-derived frontal ablation ($U_{fx}$ and $dl/dt$) as well as the sum of positive degree days (PDD) and rain. The calving season is characterized by sharp increases in ice loss with slight delay following the melt season onset. This abrupt increase corresponds with the increase in glacier velocities ($U_{fx}$) due to melt water induced basal sliding [*Iken and Bindschadler*, 1986; *Podrasky et al.*, 2012]. In most years, the glacier slightly advances first ($-dl/dt$) since there is limited calving, then retreat ($+dl/dt$) often occurs a week or two after the increased velocities. The seismic frontal ablation record often exhibit two peaks corresponding to $dl/dt$ and $U_{fx}$. Maximum calving activity is observed in August and September at the tail end of the melt season, slightly delayed to the maximum of PDDs in June/July (Figure 2c)[*Köhler et al.*, 2015]. This delay may be related to the fjord temperature maximum [*Jenkins*, 2011; *Bartholomaus et al.*, 2013; *Luckman et al.*, 2015]. The calving season continues through the autumn toward winter, approaching a minimum in February/March. This is not surprising given the relatively warm fjord temperatures through the autumn [*Luckman et al.*, 2015] and the lack of fast sea ice during these years. Interestingly, the decrease in frontal ablation toward the winter exhibits a classic exponential decay form (Figure 2f). The decay constant is largest for years when calving is largest at the end of summer as frontal ablation rates thus have to drop further to reach winter conditions. We suspect that this consistent decay nature of frontal ablation results from the evolution of the glacier basal hydrological system into a winter mode with reduced velocities from limited meltwater production and with reduced subaqueous melting due to fjord temperature decreases that occur at a relatively consistent time at the end of autumn each year.

The interannual variability of frontal ablation seems not related to the total annual sum of PDDs (Figures 2c and S8), but rather to intense warm wet events that occur with sufficient time separation. For example, Figure 2d shows the summer of 2008 with the initial summer speedup in mid-June that leads to the sharp increase in calving followed by the common enhanced summer frontal ablation. In mid-September, a combination of warmer temperatures and intense rain resulted in a 2 week period with calving that doubled the average summer fluxes. This shows clearly that intense warm wet events affect the basal hydrological system more than continuously warm fjord or air temperatures during summer (e.g., as in 2011) when the subglacial

drainage system can evolve to discharge more water through time [e.g., *Bartholomew et al.*, 2012]. During winter months, frontal ablation can vary significantly, with 1–3 week long phases of moderate calving activity, often associated with warmer periods and larger rain events. For example, Figure 2e shows 2011 with the common summer increase in frontal ablation rates, but with a small decay that reflects the warm wet autumn with lots of rain events that delayed the reduction on calving flux. In February 2012, a rather intense warm rain event caused a simultaneous small increase in the calving flux. These examples show the intricate relationship between the calving flux and rain events, which is not consistent throughout our record. Not all rain events caused an instantaneous increase in calving fluxes, similar to *O'Neel et al.* [2003]. *Burgess et al.* [2013] suggest that winter velocities are dictated by conditions at the end of the previous summer or beginning of autumn. In our record, winter frontal ablation is largest in 2001/2002, 2005/2006, 2008/2009, and 2011/2012, but does not correlate with the sum of PDDs during the previous summer. These years experience warm autumn temperatures with lots of rain events. For example, in late 2005, warm rain events continued through the winter, allowing for a higher level of frontal ablation that continued through to the 2006 melt season (Figure S8).

The rather large annual and seasonal variability of our glacier frontal ablation rates expresses the complexity of frontal ablation process affected and driven by meteorological and oceanic forces with shifting geometries of the glacier tongue. Passive seismic records enhance the possibility to further understand these processes in more detail with higher temporal resolutions. The large temporal variability shown through our records of Kronebreen exemplifies the difficulty in using small time snapshots of glacier dynamics by repeat satellite imagery to estimate annual or multiannual glacier flux [e.g., *Rignot et al.*, 2008] and stresses rather the importance of continuous estimates of glacier frontal ablation [e.g., *Schellenberger et al.*, 2015], a major potential of our passive seismic method.

## 5. Conclusions

Long, continuous observations of glacier frontal ablation with high temporal resolution independent of visibility are difficult to obtain. They are, however, essential to better understand the evolution of tidewater glaciers in relation to changing climate. We show for the first time the capability to produce continuous estimates of frontal ablation from a glacier without in situ observations by combining the passive seismic record with satellite-derived estimates. Using these calibration data, we estimated frontal ablation at Kronebreen with weekly resolution for the past 15 years, including the dark Arctic winter seasons, when visual observation cannot be made. The total frontal ablation between 2001 and 2015 amounts to 3.7–4.2 $km^3$, with the highest annual rates between September 2013 and August 2014 with 0.33–0.48 $km^3 a^{-1}$ corresponding with the heavy retreat of the glacier terminus, about 1 km until summer 2015. Our model performs best using the cumulative duration of individual seismic calving events and an indicator for the seismic calving record incompleteness that corrects for the effect of noise on seismic event detectability. The choice of this variable is motivated by the power law distribution associated with the frequency size distribution of calving events.

The long, continuous, and high-resolution frontal ablation rates reveal a number of patterns at various time scales. Calving tends to increase strongly during the characteristic summer speedup of the glacier. Calving activity contains multiple short-lived peaks, usually associated with a nonconstant delay to heavier melt and rain events. Moreover, peak calving activity occurs 1–2 months later than the peak melt season and often calving continues long into the autumn and early winter. Over our entire calving record, the decrease in calving activity in late autumn shows a characteristic decay form that with more investigation may reveal relationships with the state of the basal hydrological system at the end of the summer and/or fjord conditions. In summary, this new high-resolution record of frontal ablation opens a treasure chest for better understanding glacier dynamic feedback processes at the ice-ocean interface when further combined with additional records such as glacier surface mass balance and fjord water temperatures. Future studies should aim to calibrate the models at shorter timescales that can reveal diurnal, semidiurnal, or even hourly variations of calving.

**Acknowledgments**
This study was funded by the Research Council of Norway (project SEISMOGLAC, 213359/F20 and CalvingSEIS, 244196/E10; support from NORRUSS program, project 233973/H30). We use ObsPy [*Beyreuther et al.*, 2010] and EP/DP [*Fyen*, 1989; *Schweitzer et al.*, 2012] software for seismic data analysis, and Python packages "statsmodel" [*Seabold and Perktold*, 2010] for GLMs and "scikit-learn" [*Pedregosa et al.*, 2011] for Bayes classifiers. Figures are produced using GMT [*Wessel and Smith*, 1998]. Local seismic instrumentation was provided by the Geophysical Instrument Pool of GFZ Potsdam, Germany, and University of Kiel, Germany. E.B. acknowledges support from CNES through the TOSCA and ISIS programs. C.N. acknowledges funding from European Union/ERC (grant 320816) and ESA (project Glaciers CCI, 4000109873/14/I-NB). Supporting information provide access to data (Data Set S1/S2 and Text S1). We thank Timothy Bartholomaus and Fabian Walter for their reviews.

## References

Amundson, J. M., M. Truffer, M. P. LÃijthi, M. Fahnestock, M. West, and R. J. Motyka (2008), Glacier, fjord, and seismic response to recent large calving events, Jakobshavn Isbræ, Greenland, *Geophys. Res. Lett.*, *35*(22), L22501, doi:10.1029/2008GL035281.

Asming, V., and A. Fedorov (2015), Possibility of using a single three-component station automatic detector–locator for detailed seismological observations, *Seismic Instrum.*, *51*(3), 201–208, doi:10.3103/S0747923915030032.

Asming, V., E. Kremenetskaya, Y. Vinogradov, and A. Fedorov (2015), On usage of naive Bayesian classifiers in seismology, *Seismic Instrum.*, *51*(4), 22–28.

Åström, J. A., et al. (2014), Termini of calving glaciers as self-organized critical systems, *Nature Geosci.*, *7*(12), 874–878, doi:10.1038/ngeo2290.
Bahr, K. (2015), High resolution glacier dynamics from GNSS measurements on Holtedahlfonna, NW Svalbard, Master's Thesis, Univ. Oslo.
Bartholomaus, T., C. Larsen, S. O'Neel, and M. West (2012), Calving seismicity from iceberg–sea surface interactions, *J. Geophys. Res.*, *117*(F4), F04029, doi:10.1029/2012JF002513.
Bartholomaus, T. C., C. F. Larsen, and S. O'Neel (2013), Does calving matter? Evidence for significant submarine melt, *Earth Planet. Sci. Lett.*, *380*, 21–30, doi:10.1016/j.epsl.2013.08.014.
Bartholomaus, T. C., C. F. Larsen, M. E. West, S. O'Neel, E. C. Pettit, and M. Truffer (2015), Tidal and seasonal variations in calving flux observed with passive seismology, *J. Geophys. Res. Earth Surface*, *120*(11), 2318–2337, doi:10.1002/2015JF003641.
Bartholomew, I., P. Nienow, A. Sole, D. Mair, T. Cowton, and M. A. King (2012), Short-term variability in Greenland ice sheet motion forced by time-varying meltwater drainage: Implications for the relationship between subglacial drainage system behavior and ice velocity, *J. Geophys. Res.*, *117*(F3), F03002, doi:10.1029/2011JF002220.
Benn, D. I., C. R. Warren, and R. H. Mottram (2007), Calving processes and the dynamics of calving glaciers, *Earth Sci. Rev.*, *82*(3–4), 143–179, doi:10.1016/j.earscirev.2007.02.002.
Beyreuther, M., R. Barsch, L. Krischer, T. Megies, Y. Behr, and J. Wassermann (2010), ObsPy: A Python toolbox for seismology, *Seismol. Res. Lett.*, *81*(3), 530–533, doi:10.1785/gssrl.81.3.530.
Bishop, C. M. (2006), *Pattern Recognition and Machine Learning*, Springer Inc., New York.
Burgess, E. W., R. R. Forster, and C. F. Larsen (2013), Flow velocities of Alaskan glaciers, *Nat. Commun.*, *4*(2146), 1–8, doi:10.1038/ncomms3146.
Chapuis, A., and T. Tetzlaff (2014), The variability of tidewater-glacier calving: Origin of event-size and interval distributions, *J. Glaciol.*, *60*(222), 622–634, doi:10.3189/2014JoG13J215.
Chapuis, A., C. Rolstad, and R. Norland (2010), Interpretation of amplitude data from a ground-based radar in combination with terrestrial photogrammetry and visual observations for calving monitoring of Kronebreen, Svalbard, *Ann. Glaciol.*, *51*(55), 34–40, doi:10.3189/172756410791392781.
Cogley, J., et al. (2011), Glossary of glacier mass balance and related terms, *IHP-VII Tech. Documents in Hydrology No. 86*, IACS Contribution No. 2, UNESCO-IHP, Paris.
Ekström, G., M. Nettles, and G. A. Abers (2003), Glacial earthquakes, *Science*, *302*(5645), 622–624, doi:10.1126/science.1088057.
Flinn, E. (1965), Signal analysis using rectilinearity and direction of particle motion, *Proc. IEEE*, *53*(12), 1874–1876, doi:10.1109/PROC.1965.4462.
Fyen, J. (1989), Event processor program package, *NORSAR Semiannual Tech. Summary, NORSAR Scientific Rep. 2–88/89*, 117–123, NORSAR, Kjeller, Norway.
Gardner, A. S., et al. (2013), A reconciled estimate of glacier contributions to sea level rise: 2003 to 2009, *Science*, *340*(6134), 852–857, doi:10.1126/science.1234532.
Huss, M., and R. Hock (2015), A new model for global glacier change and sea-level rise, *Front. Earth Sci.*, *3*(54), doi:10.3389/feart.2015.00054.
Iken, A., and R. A. Bindschadler (1986), Combined measurements of subglacial water pressure and surface velocity of Findelengletscher, Switzerland: Conclusions about drainage system and sliding mechanism, *J. Glaciol.*, *32*(110), 101–119, doi:10.3198/1986JoG32-110-101-119.
Jenkins, A. (2011), Convection-driven melting near the grounding lines of ice shelves and tidewater glaciers, *J. Phys. Oceanogr.*, *41*(12), 2279–2294, doi:10.1175/JPO-D-11-03.1.
Kääb, A., B. Lefauconnier, and K. Melvold (2005), Flow field of Kronebreen, Svalbard, using repeated Landsat 7 and ASTER data, *Ann. Glaciol.*, *42*(1), 7–13, doi:10.3189/172756405781812916.
Köhler, A., A. Chapuis, C. Nuth, J. Kohler, and C. Weidle (2012), Autonomous detection of calving-related seismicity at Kronebreen, Svalbard, *The Cryosphere*, *6*, 393–406, doi:10.5194/tc-6-393-2012.
Köhler, A., C. Nuth, J. Schweitzer, C. Weidle, and S. J. Gibbons (2015), Regional passive seismic monitoring reveals dynamic glacier activity on Spitsbergen, Svalbard, *Polar Res.*, *34*, 26178, doi:10.3402/polar.v34.26178.
Korona, J., E. Berthier, M. Bernard, F. Rémy, and E. Thouvenot (2009), SPIRIT. SPOT 5 stereoscopic survey of Polar Ice: Reference images and topographies during the fourth International Polar Year (2007–2009), *ISPRS J. Photogramm. Remote Sens.*, *64*(2), 204–212, doi:10.1016/j.isprsjprs.2008.10.005.
Koubova, H. (2015), Localization and analysis of calving-related seismicity at Kronebreen, Svalbard, Master's Thesis, Univ. of Oslo.
Leprince, S., S. Barbot, F. Ayoub, and J.-P. Avouac (2007), Automatic and precise orthorectification, coregistration, and subpixel correlation of satellite images, application to ground deformation measurements, *IEEE Trans. Geosci. Remote Sens.*, *45*(6), 1529–1558, doi:10.1109/TGRS.2006.888937.
Luckman, A., D. I. Benn, F. Cottier, S. Bevan, F. Nilsen, and M. Inall (2015), Calving rates at tidewater glaciers vary strongly with ocean temperature, *Nat. Commun.*, *6*(8566), doi:10.1038/ncomms9566.
Mansell, D., A. Luckman, and T. Murray (2012), Dynamics of tidewater surge-type glaciers in northwest Svalbard, *J. Glaciol.*, *58*(207), 110–118, doi:10.3189/2012JoG11J058.
McCullagh, P., and J. A. Nelder (1989), *Generalized Linear Models*, vol. 37, CRC press, London, New York.
Nuth, C., T. V. Schuler, J. Kohler, B. Altena, and J. O. Hagen (2012), Estimating the long-term calving flux of Kronebreen, Svalbard, from geodetic elevation changes and mass-balance modelling, *J. Glaciol.*, *58*(207), 119–133, doi:10.3189/2012JoG11J036.
Nuth, C., J. Kohler, M. König, A. von Deschwanden, J. Hagen, A. Kääb, G. Moholdt, and R. Pettersson (2013), Decadal changes from a multi-temporal glacier inventory of Svalbard, *The Cryosphere*, *7*, 1603–1621, doi:10.5194/tc-7-1603-2013.
Ogata, Y., and K. Katsura (1993), Analysis of temporal and spatial heterogeneity of magnitude frequency distribution inferred from earthquake catalogues, *Geophys. J. Int.*, *113*(3), 727–738, doi:10.1111/j.1365-246X.1993.tb04663.x.
Ohrnberger, M., E. Schissele, C. Cornou, S. Bonnefoy-Claudet, M. Wathelet, A. Savvaidis, F. Scherbaum, and D. Jongmans (2004), Frequency wavenumber and spatial autocorrelation methods for dispersion curve determination from ambient vibration recordings, in *Proceedings of the 13th World Conference on Earthquake Engineering*, pp. 946, WCEE, Vancouver, Canada.
O'Neel, S., and W. T. Pfeffer (2007a), Source mechanics for monochromatic icequakes produced during iceberg calving at Columbia Glacier, AK, *Geophys. Res. Lett.*, *34*(22), L22502, doi:10.1029/2007GL031370.
O'Neel, S., K. A. Echelmeyer, and R. J. Motyka (2003), Short-term variations in calving of a tidewater glacier: LeConte Glacier, Alaska, U.S.A., *J. Glaciol.*, *49*(167), 587–598, doi:10.3189/172756503781830430.
O'Neel, S., H. P. Marshall, D. E. McNamara, and W. T. Pfeffer (2007b), Seismic detection and analysis of icequakes at Columbia Glacier, Alaska, *J. Geophys. Res.*, *112*, F03S23, doi:10.1029/2006JF000595.

O'Neel, S., C. Larsen, N. Rupert, and R. Hansen (2010), Iceberg calving as a primary source of regional-scale glacier-generated seismicity in the St. Elias Mountains, *J. Geophys. Res.*, *115*, F04034, doi:10.1029/2009JF001598.
Pedregosa, F., et al. (2011), Scikit-learn: Machine learning in Python, *J. Mach. Learn. Res.*, *12*, 2825–2830.
Podolskiy, E. A., and F. Walter (2016), Cryo-seismology, *Rev. Geophys.*, *54*, 1–43, doi:10.1002/2016RG000526.
Podrasky, D., M. Truffer, M. Fahnestock, J. M. Amundson, R. Cassotto, and I. Joughin (2012), Outlet glacier response to forcing over hourly to interannual timescales, Jakobshavn Isbræ, Greenland, *J. Glaciol.*, *58*(212), 1212–1226, doi:10.3189/2012JoG12J065.
Qamar, A. (1988), Calving icebergs: A source of low-frequency seismic signals from Columbia Glacier, Alaska, *J. Geophys. Res.*, *93*(B6), 6615–6623, doi:10.1029/JB093iB06p06615.
Richardson, J. P., G. P. Waite, K. A. FitzGerald, and W. D. Pennington (2010), Characteristics of seismic and acoustic signals produced by calving, Bering Glacier, Alaska, *Geophys. Res. Lett.*, *37*(3), L03503, doi:10.1029/2009GL041113.
Rignot, E., J. Box, E. Burgess, and E. Hanna (2008), Mass balance of the Greenland ice sheet from 1958 to 2007, *Geophys. Res. Lett.*, *35*, L20502, doi:10.1029/2008GL035417.
Schellenberger, T., T. Dunse, A. Kääb, J. Kohler, and C. Reijmer (2015), Surface speed and frontal ablation of Kronebreen and Kongsbreen, NW Svalbard, from SAR offset tracking, *The Cryosphere*, *9*(6), 2339–2355, doi:10.5194/tc-9-2339-2015.
Schweitzer, J., J. Fyen, S. Mykkeltveit, S. Gibbons, M. Pirli, D. Kühn, and T. Kværna (2012), Seismic Arrays, in *New Manual of Seismological Observatory Practice (NMSOP-2)*, 2nd edn., edited by P. Bormann, pp. 1–80, Potsdam: Deutsches GeoForschungsZentrum GFZ.
Seabold, S., and J. Perktold (2010), Statsmodels: Econometric and statistical modeling with python, in *Proceedings of the 9th Python in Science Conference*, pp. 57–61, Austin, Tex.
Vaughan, D., et al. (2013), Observations: Cryosphere, in *Panel on Climate Change*, edited by T. F. Stocker et al., Cambridge Univ. Press Cambridge, U. K., and New York.
Vieli, A., and F. M. Nick (2011), Understanding and modelling rapid dynamic changes of tidewater outlet glaciers: Issues and implications, *Surv. Geophys.*, *32*(4), 437–458.
Voigt, U. (1966), The determination of the direction of movement on glacier surfaces by terrestrial photogrammetry, *J. Glaciol.*, *6*, 359–367, doi:10.3198/1966JoG6-46-359-367.
Walter, F., J. M. Amundson, S. O'Neel, M. Truffer, M. Fahnestock, and H. A. Fricker (2012), Analysis of low-frequency seismic signals generated during a multiple-iceberg calving event at Jakobshavn Isbræ, Greenland, *J. Geophys. Res.*, *117*(F01036), doi:10.1029/2011JF002132.
Wessel, P., and W. H. F. Smith (1998), New, improved version of GMT released, *Eos, Trans. AGU*, *79*(47), 579–579, doi:10.1029/98EO00426.
Woessner, J., and S. Wiemer (2005), Assessing the quality of earthquake catalogues: Estimating the magnitude of completeness and its uncertainty, *Bull. Seismol. Soc. Am.*, *95*(2), 684–698, doi:10.1785/0120040007.